Challenging Glass 6 - Conference on Architectural and Structural Applications of Glass
Louter, Bos, Belis, Veer, Nijsse (Eds.), Delft University of Technology, May 2018.

ISBN 978-94-6366-044-0, https://doi.org/10.7480/cgc.6.2184

Stability of Dry-Stacked Glass Masonry Arch Bridges

Chris Noteboom [a], Mike Aurik [a, b], Ate Snijder [b]
[a] *Arup, The Netherlands, chris.noteboom@arup.com*
[b] *TU Delft, Faculty of Architecture and the Built Environment,, The Netherlands*

The plan of the glass group of the TU Delft to realize a 14m span dry-stacked glass arched masonry bridge led to investigation of stability of glass arches in more general. Analytical and numerical analysis are done to compare results. Analytical analyses are based on methods developed for traditional stone arches. A graph is plotted in which the relationship between rise-to-span ratio and thickness-to-span ratio is derived and presented such that the relevant instability mechanism(s) can be determined. The required thickness of a stable arch can be found by applying a geometrical factor of safety. To investigate 2nd order effects and stresses, finite element models are presented. The models verify the analytical solutions and are used to investigate the influence of axial stiffness and nonlinear effects on stability.

Keywords: Glass, Arch, Stability

1. Introduction

The glass group of the TU Delft has plans to realize a 14m span dry-stacked glass arched masonry bridge. The bridge is planned to be constructed at the TU Delft campus and will mark the entrance to the 'Green Village' innovation park. The glass group of the TU Delft gained experience with glass masonry structures by contributing significantly to the realization of the Crystal Houses, located at the P.C. Hooftstraat in Amsterdam. This 10m high glass masonry façade that features buttresses for out of plane stiffness is further described by Oikonomopoulou (2014).

Applications of solid glass bricks are quite rare, but most projects apply transparent adhesive in between glass bricks to create structural masonry. As in the Crystal Houses project, the Atocha memorial in Madrid uses an UV hardening transparent acrylate to connect the glass (Lomholt, 2007). However, the concept for the 14m span glass arched masonry bridge, is to design for disassembly and this is very difficult when adhesive connections are applied. As the bridge is designed with an arch shape, mainly normal forces instead of shear forces are transferred in between bricks. Therefore, the connection is designed without need for any bonding. For local shear transfer, an interlocking shape is investigated in Snijder et al. (2016) and in Bristogianni et al. (2017). A staggered arrangement of the bricks is proposed to provide lateral stability. A circular bridge shape was adopted to simplify glass brick production. Circular arches can be constructed with equal segments and therefore, in theory, only one mold is necessary to create all glass bricks.

The rise of the 14m span bridge is relatively low compared to most stone masonry arches, as the glass arch directly serves as deck limiting the slope of the arch. The low rise results in high normal forces and therefore increases the need for stability assessment.

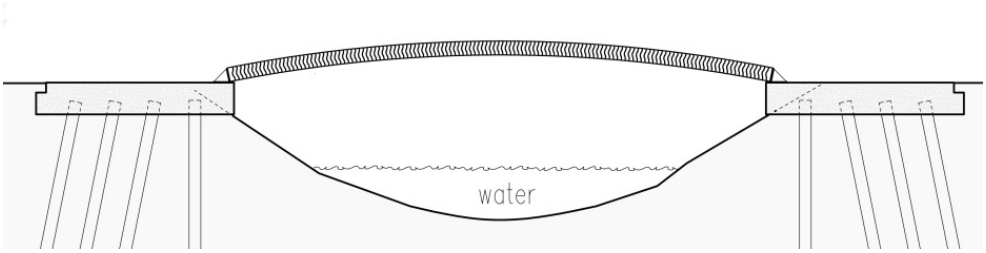

Fig. 1 Schematic representation of glass masonry bridge TU Delft campus.

In the first section of this paper, the stability of dry-stacked arch bridges is investigated analytically. Based on theory developed for traditional stone masonry arches, the relationship between rise-to-span ratio and minimum required thickness is explored. A graph is plotted in which instability mechanisms due to support settlements and asymmetric loading are integrated. It can be used in the design stage to see what mechanisms need to be investigated and in what cases the arch is stable. In the second section, the stability is investigated numerically. Results are compared with the analytical study and a parameter analysis is done to explore the possibilities of glass masonry arches.

2. Analytical stability assessment

2.1. General

Elastic in-plane stability of arches with infinite stiff supports can be easily assessed with the Euler-Yasinki formula: $F_{buc}=\pi^2EI/(0{,}25L_{arch}^2)$ (Gambhir, 2004). This formula is based on the assumption of a continuous beam in which compression, tension and shear forces can be transferred over the full cross section. However, dry stacked arches are based on the principle of compression-only transfer between bricks. Dry stacked masonry is stable when the resultant of the forces lies within the boundaries of the masonry; between the extrados (upper surface) and the intrados (lower surface).

The analytical assessment of the stability of traditional stone masonry is described by Heyman (1995). The main assumptions are: (1) infinite compression strength, (2) no tensile strength and (3) sliding failure does not occur. These same assumptions are used for the analytical investigation of the glass masonry bridge. This implies that very high compressive stresses may occur, which would realisticly lead to local crushing of the glass. It is assumed that this has minor impact on stability and the investigation of stresses is outside the scope of this paper.

Masonry arches are regarded as hyperstatic structures. Very small imposed displacements or imperfections will influence the 'actual' position of the line of trust. Although the working state is unknown, if the structure is loaded slowly to collapse, the maximum load is not influenced by the current working state. This is standard practice for all structures and limit state design. If the designer of a dry stacked masonry arch is able to construct the line of trust within the boundaries of the arch it is stable. For a safe design, a geometrical safety factor is applied to the arch's minimum thickness. Similar to steel structure analysis, plastic hinges are allowed if these do not compromise the stability (Heyman, 1995). Although stone or glass is not ductile in itself, it may be regarded as ductile when applied as masonry. The ductile response is a result of cracks that may slowly develop in between the bricks.

2.2. Support settlements

Up to a certain level, an arch is able to accommodate the supports settlements. If they become sufficiently large however, the arch becomes unstable due to the formation of a mechanism. Which failure mechanism occurs, depends on the geometry. Based on the failure behaviour concerning settlements, three geometry-regions may be distinguished. These regions are illustrated in Fig. 2. Fig. 2a shows the results of the derivations in this paragraph and 2b shows the failure mechanisms. Region A indicates arches which fail by a 3-hinge snap-through mechanism and has stationary hinges. Region C indicates arches that fail by a 5-hinge mechanism. In this region the hinges will shift during the settlements, to accommodate for the changes in the line of thrust. Region B indicates a `transition zone'. In this region the hinges will not move up until the point that the line of thrust becomes tangent to the geometry at the location of the supports.

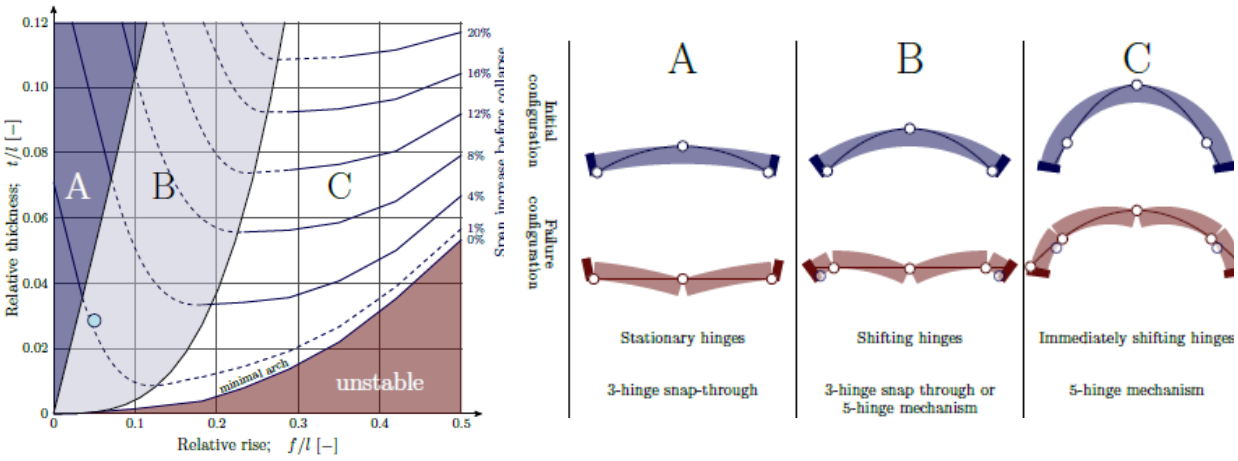

a) b)

Fig. 2a) Region definitions in which the dot indicates the geometry of the TU Delft masonry glass bridge; 2b) Failure mechanism for each region.

The A-B-boundary was found by Oschendorf (2002) and is rewritten in a different geometry-notation (Fig. 3):

$$\frac{t}{l} = \frac{2(1-\cos\beta)}{1+\cos\beta)}\frac{1}{2\sin\beta} \tag{1}$$

$$\beta = \sin^{-1}\frac{f/l}{(f/l)^2+\frac{1}{4}} \tag{2}$$

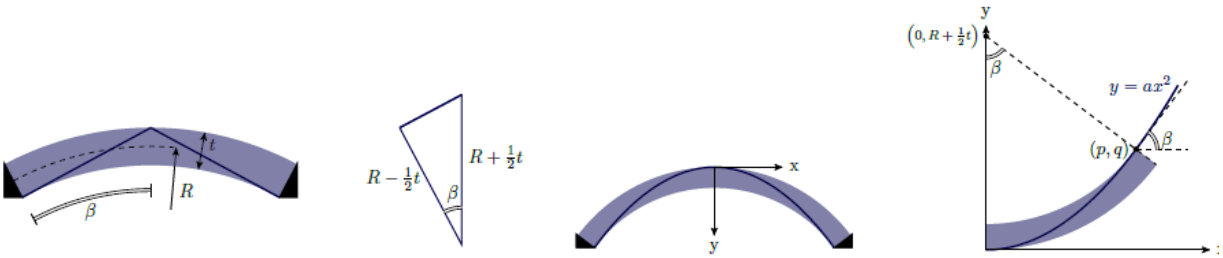

a) b)

Fig. 3 Geometry definitions for analytical derivation; a) boundary between region A and B; b) boundary between region B and C.

An arch at the boundary of region B and C, has a parabolic line of trust that is tangential at the supports, as illustrated in Fig. 2b. To provide an expression for this boundary, the coordinate system is chosen such that its origin is located in the vertex of the parabola. It must hold that the slope of the parabola is equal to the slope of the intrados, at the indicated coordinate (p,q). This provides the following equation:

$$\frac{2q}{p} = tan\,\beta \tag{3}$$

The coordinates p and q are given by the following expressions:

$$p = (R - \tfrac{1}{2}t)\,cos(-90 + \beta) \tag{4}$$

$$q = R + \tfrac{1}{2}t + (R - \tfrac{1}{2}t)\,sin(-90 + \beta) \tag{5}$$

Substituting (4) and (5) in equation (3) and simplifying the result, provides the following definition of the boundary between region B and C:

$$\frac{R+\frac{1}{2}t}{R-\frac{1}{2}t}\cos\beta = 1 - \tfrac{1}{2}sin\,\beta^2 \tag{6}$$

The percentage that the span of an arch can increase before it collapses, is indicated by the contour lines of Fig. 2a. The failure mechanism that arises due to settlements, differs per region. Therefore, also the trajectory of the contour lines does. The part of the contour lines that is located in region A, follows from an analytical relation. Region B can be considered as a transition zone and will be investigated as well. For region C the contour lines have been derived using results found in literature.

The five-hinge collapse mechanism corresponding to region C, was investigated by Oschendorf (2002). The investigation depended on an iterative model, validated by some physical experiments. The results were used to construct (the non-dashed part of) the contour lines in region C.

The effect of settlements can be assessed using rigid body kinematics. Assuming an infinite stiffness, hinges will directly be formed when settlements start to occur. They will be located at the supports and in the middle of the arch. Instability in the form of a snapthrough mechanism will occur as soon as the hinges are on a horizontal line. The vertical distance between the hinges, z may be expressed as a function of the total displacement u. Using Fig. 4, the following formula may be derived:

$$z(u) = \tfrac{1}{2}\sqrt{l^2 + (2f + 2t)^2 - (l + u)^2} \tag{7}$$

The contour lines of 2a, indicate the span increase percentage till collapse. For region A these contour lines can be derived by substituting l+u = ξl and z = 0 in equation (7). The variable ξ is the span increase factor at the moment of collapse, i.e. for a span increase percentage of 2%, this factor equals ξ = 1.02. The contour lines are defined by the following formula:

$$\frac{t}{l} = -\frac{f}{l} + \tfrac{1}{2}\sqrt{\xi^2 - 1} \tag{8}$$

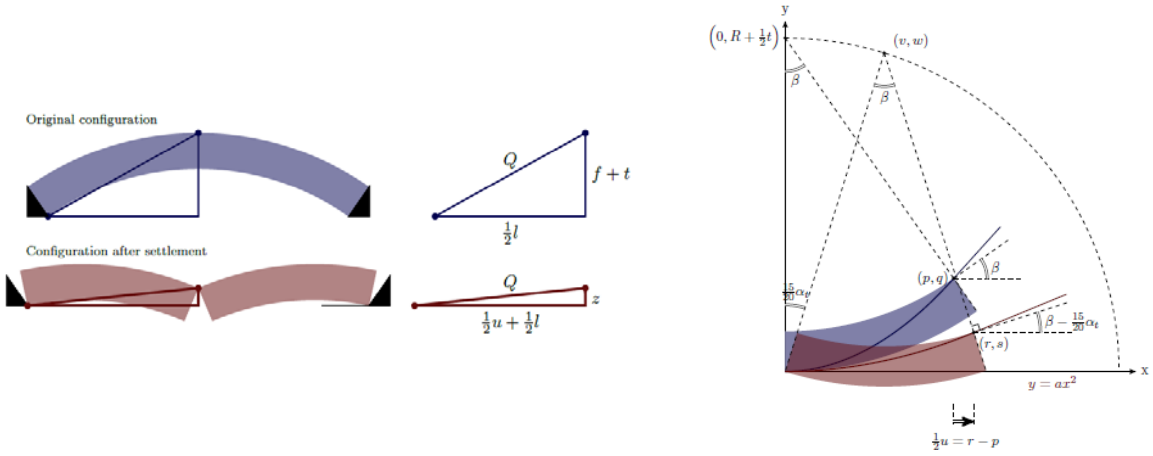

a) b)

Fig. 4 Fig.s for analytical analysis of settlements; a) rigid body movement for settlement analysis region A; b) geometry definition to analyze settlement when line of thrust becomes tangent with intrados (region B).

An arch in region B initially behaves the same as one in region A. Thus, the hinges will initially be located at the supports and in the middle. This means that the same rigid body movement occurs, as expressed by formula (7). After a certain settlement however, the line of thrust will be tangent to the intrados of the arch. At this point the outer hinges will start to shift to the middle, similar as to what happens in region C. Increasing the settlements further, will finally result in collapse.

So up to a certain limit, formula (8) can be used for region B as well. The settlement corresponding to this limit, is determined. To reduce complexity of the derivation, the coordinate system is conveniently chosen and the parameters R, and t are used to express the geometry of the arch (Fig. 4b). The line of thrust is tangent to the intrados after the circle segment has rotated by an angle α_t.

The expressions for the coordinates can be derived using Fig. 4b:

$$p = (R - \tfrac{1}{2}t)\, cos(-90 + \beta) \tag{9}$$

$$q = R + \tfrac{1}{2}t + (R - \tfrac{1}{2}t)\, sin(-90 + \beta) \tag{10}$$

$$v = (R + \tfrac{1}{2}t)\, cos(90 - \alpha_t) \tag{11}$$

$$w = (R + \tfrac{1}{2}t)\, sin(90 - \alpha_t) \tag{12}$$

$$r = v + (R - \tfrac{1}{2}t)\, cos(-90 - \alpha_t + \beta) \tag{13}$$

$$s = w + (R - \tfrac{1}{2}t)\, sin(-90 - \alpha_t + \beta) \tag{14}$$

After a rotation α_t, the line of thrust can be defined by a parabola of the form $y = ax^2$, intersecting the point (r,s). This means that $a = s/r^2$. The slope of the line of thrust at the support can be found by computing the derivative in point (r,s).

$$y'(x) = 2ax = \frac{2s}{r^2} \tag{15}$$

$$y'(r) = \frac{2a}{r} \tag{16}$$

This slope must be equal to the slope of the intrados, which provides the following equation:

$$\frac{2a}{r} = tan(\beta - \alpha_t) \tag{17}$$

Using this equation, the angle α_t can be computed. The result can be used to compute all relevant coordinates. The coordinates can be used to determine the settlement for which the line of thrust becomes tangent and the hinges will start to shift.

$$u = 2(r - p) \tag{18}$$

For an arch close to the boundary with region A, the settlement-boundary is close to the maximum settlement. Therefore this arch behaves almost entirely the same as an arch in region A. By moving away from this boundary, the behavior will start to deviate. Similarly an arch close to the boundary with region C behaves almost entirely the same as an arch in region C. Therefore it is expected that the contour lines in region B, illustrated in Fig. 2a are tangent at both region boundaries. Based on these considerations, the dashed part of the contour lines have been drawn.

The analytical derivation shown before and regions in Fig. 2a are based on the assumption that the arch is infinitely stiff and that settlements are independent of support reactions. However, if settlements depend on the horizontal reaction force of the arch, a nonlinear effect should be included. This can be done via an iterative calculation.

2.3. Asymmetric loads

Under its self-weight, an arch has a symmetric line of thrust. An external asymmetric load causes a disturbance in the line of thrust, which may result in a four-hinge mechanism. For certain geometries the stability can be guaranteed independent of the external load. The most unfavorable scenario would be the application of a large point load at a certain position along the span. If a horizontal line can be contained within the geometry, as shown in Fig. 5, the line of thrust is allways contained within the geometry. This is called an 'unconditionally stable arch' as for every asymmetric load it is stable. The geometry is then defined by the following requirement:

$$\beta \leq arccos\left(\frac{1-\frac{t}{2R}}{1+\frac{t}{2R}}\right) \tag{19}$$

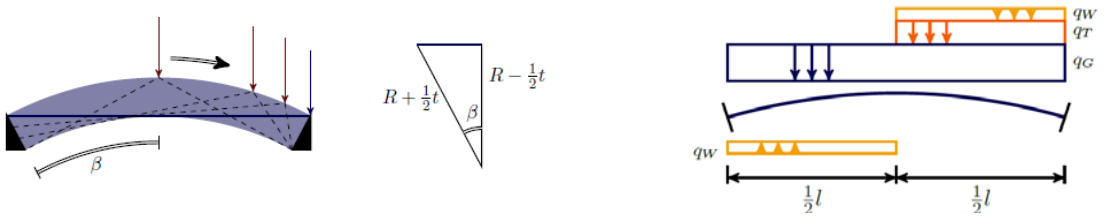

a) b)

Fig. 5; a) Definition of an unconditionally stable arch; b) example of line of thrust with four hinges.

In case of asymmetric loading and a geometry that is not 'unconditionally stable' an analysis should be performed to determine if it is stable, by checking if its thickness is sufficiently large.

There is a minimal thickness for which the line of trust can be contained within the geometry of the arch. For this minimal arch, only one position for the line of thrust can be constructed. The structure is now at the boundary of collapse and any slight imperfection will cause collapse. In order to increase the safety, the thickness of the arch is increased by a factor 2 that is used in practice. This is is sufficient to account for construction imperfections, slight settlements and temperature loads. (Heyman 1995).

A possible position for the line of thrust may be found by computing the elastic solution based on the 'beam + inverted cable'-system. The horizontal support reaction in this analysis is based on the elastic properties of the arch. For the assymetrical crowd load configuration, as shown in Fig. 5b, the following differential equations are used:

$$EI\frac{d^4w_A}{dx^4} + H\frac{d^2z}{dx^2} = q_A(x) \quad for -\frac{1}{2}l \leq x \leq 0 \tag{20}$$

$$EI\frac{d^4w_B}{dx^4} + H\frac{d^2z}{dx^2} = q_B(x) \quad for \quad 0 \leq x \leq \frac{1}{2}l \tag{21}$$

These differential equations represent the ‘beam + inverted cable’-system, where z(x) represents the position of the arch and are ased on the assumption that the rise/span ratio is relatively low. A distinction between two domains is made as a result of the discontinuity in loading. Solving the differential equations, provides the excentricity and the position of the line of thrust, at any given location x:

$$e_A(x) = -\frac{1}{2}\frac{(q_A - q_B)(8x^2 + 3lx)f}{(q_A + q_B)l^2} \qquad z_A(x) = z(x) + e_A(x) \tag{22}$$

$$e_B(x) = -\frac{1}{2}\frac{(q_A - q_B)(-8x^2 + 3lx)f}{(q_A + q_B)l^2} \qquad z_B(x) = z(x) + e_B(x) \tag{23}$$

The assymetrical load ‘disturbes’ the position of the line of thrust. The disturbance depends on the ratio between the assymetrical load, and the symmetrical dead load. For a 14m span arch, the line of thrust is computed using equations (22) and (23) as shown in Fig. 6a. The thickness of this arch is now decreased, until the line of thrust touches the boundaries, meaning 4 hinges are formed and the structure is at the boundary of collapse. Note that reducing the thickness, also reduces the self weight. This means that the eccentricity of the line of thrust will increase.

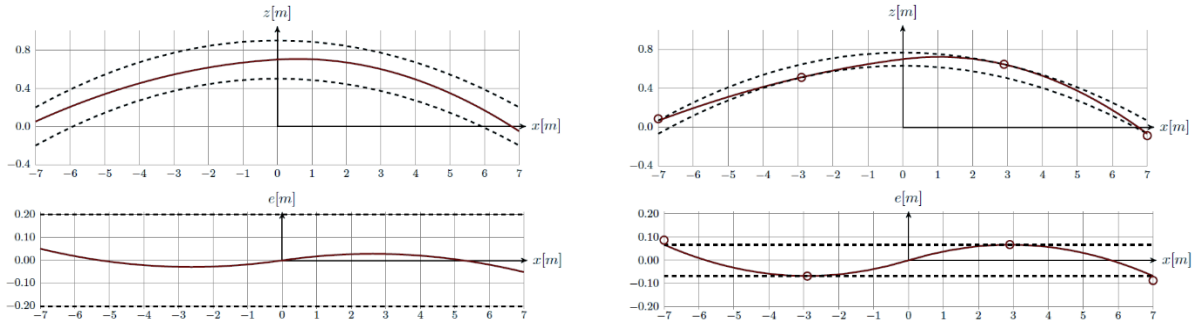

a) b)

Fig. 6 Line of thrust under an asymmetrical crowd load; a)For an arch with a certain thickness; b) After reducing the thickness to the minimal thickness, such that four hinges are formed and the arch is at the boundary of collapse.

The analysis on the 14m span example above, has also been executed for several spans and rise/span ratio’s. For each case the required deck thickness was computed, that corresponds to a geometrical safety factor of 2. The analysis was done for the load scenario shown in Fig. 5b, with an asymmetrical crowd load in accordance with the NEN-EN 1991. The result, which is given in Fig. 7a, can be used to estimate the required deck thickness for a given span and rise/span ratio.

2.4. Design graphs

The design curves for asymmetric load conditions to determine the dry stacked glass thickness as derived in the previous paragraph and shown in Fig. 7a can be used together with the general design graph shown in Fig. 7b. The latter graph is a modified version from the graph in Fig. 2a to distinguish 4 stability-related regions:

- Region I: Stability is guaranteed for both asymmetric load conditions and support settlements;
- Region II: Stability is guaranteed for asymmetric load (unconditionally stable), but support settlements need to be checked.
- Region III: Stability is guaranteed for support settlements up to 4%, but asymmetric loading should be investigated (i.e. use Fig. 7a).
- Region IV: Stability should be investigated for both asymmetric load and support settlements.

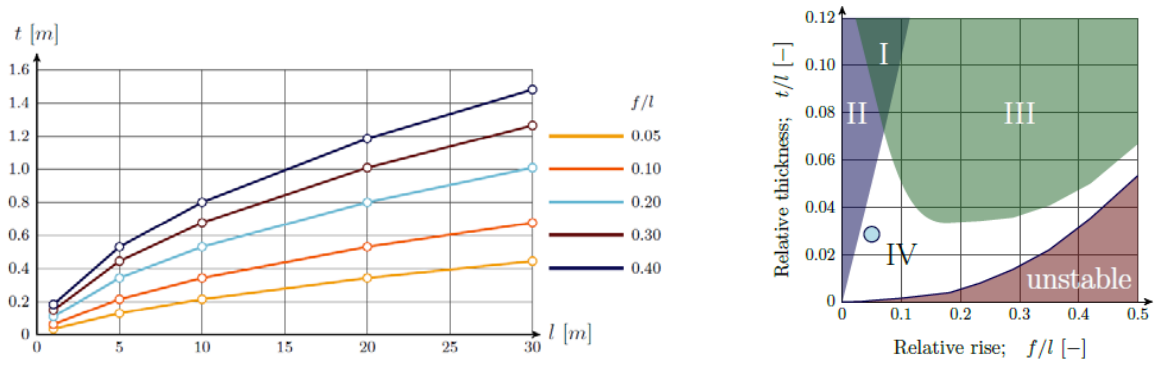

a) b)

Fig. 7 Design graphs for dry-stacked glass masonry bridges; a) Required deck thickness as a function of the span, for several f/l-ratios; based on a geometrical safety factor of 2 and an asymmetrical crowd load, in accordance with the NEN-EN 1991; b) General geometry categories for stability. The blue dot indicates the geometry of the TU Delft bridge.

3. Numerical stability assessment

The analytical investigation of the stability of masonry glass arches described in this paper is based on a simplified structure to be able to understand the influence of geometry on failure mechanisms. However, it does not consider the following relevant conditions:

- the combined effect of asymmetric loading and support settlements;
- axial stiffness;
- support stiffness.

Without consideration of these effects the critical horizontal displacement of the supports is independent of scale; only the ratios t//l and f/l are relevant. In this section the implications will be investigated by means of finite element (FE) models. First, the FE model is described. Second, the model is run without asymmetric loading and relatively high axial stiffness to verify that the analytical and numerical method match. Third, the effects of axial stiffness and asymmetric loading are considered.

3.1. Materials: Setup of numerical model

A 2D model is set up in FE software Diana. The analysis is physical and geometrical non-linear. Proportions of the TU Delft Glass Arch Bridge are the basis for the models: *span (l) = 14m; height (f) = 0.7m; deck thickness (t) = 0.4m.* Material properties are specified in table 1.

Table 1: Material properties glass.

	Glass	Unit
Young's modulus	70	GPa
Poisson's ration	0.2	-
Mass density	25.0	kN/m^3

The arch is divided in 140 glass bricks and between every brick an interface without tensile capacity is applied to model the 'dry stacking'. Once tensile stresses occur, axial and transversal stiffness between adjacent elements is set to zero. The element size therefore determines how cracks develop. Interface propoerties are specified in table 2.

Table 2: Properties interface.

	Interface	Unit
Axial stiffness modulus (E/t)	$3.0 \cdot 10^{10}$	N/m^3
Shear stiffness modulus	$3.0 \cdot 10^{10}$	N/m^3
Tensile strength	$1.0 \cdot 10^{-4}$	N/m^2
Interface nonlinearities	Discrete Cracking	-
Tensile strength after cracking	0	N/m^2
Shear stiffness after cracking	0	N/m^3

Translation is prevented at one edge of the end bricks to model the supports as shown in Fig. 8b. This simplistic way of modeling of the supports is not critical as the first interface can only transfer compression forces and has a limited stiffness. However, it should be noted that the span reduces slightly due to this way of modeling.

To investigate snap-through, load is applied in load steps. In the first load step dead load is applied to the model. In the following load steps imposed displacement is applied to the supports in steps of 0.2 mm. Failure of the arch is defined here as when the solver is unable to converge. At this point, the applied imposed displacement to the supports approaches the real 'critical' settlement at which snap-through will occur.

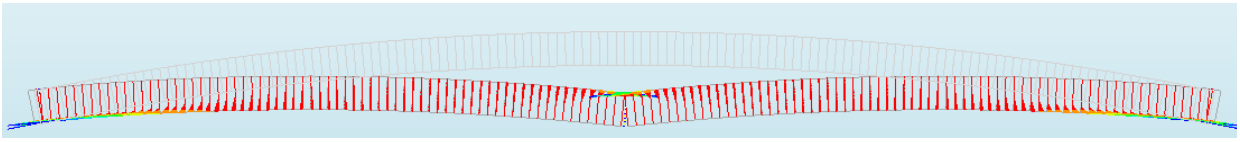

a)

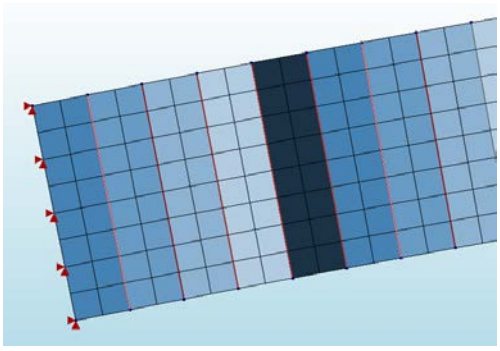

b)

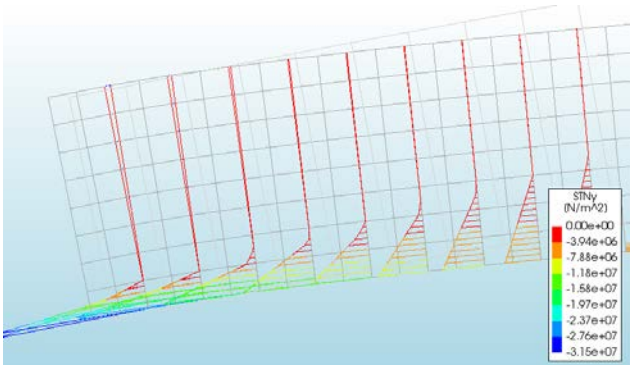

c)

Fig. 8 Fig.s of the 2D finite element model, a) global view with deformation just before snap-through; b) supports at end of arch; c) support section view with stresses in interfaces just before snap-through.

3.2. Results: Comparing FEM to analytical model

To be able to verify the analytical solutions a very high axial stiffness is modeled and symmetric load is applied. An infinite elasticity cannot be modelled by the FE program. Therefore, the axial stiffness of the base model (t = 400mm) is gradually increased. In this way, the influence of axial stiffness on the snap-through mechanism can also be shown. Both the stiffness of the glass and the interlayer (interface) are increased as shown in table below. The two tables below show the results from 2 models; one with arch thickness of 400mm and one of 800mm (scaled by factor 2).

Table 3 Results increasing axial stiffness for t=400mm model

Multiplication factor axial stiffness	E glass [N/m^2]	E/t int [N/m^3]	Critical displacement Support. [mm]	Total crit displ as % of span.
1	7.00E+10	3.00E+10	44.40	0.63
10	7E+11	3.00E+11	60.20	0.86
20	1.4E+12	6.00E+11	66.80	0.95
30	2.1E+12	9.00E+11	69.35	0.99
40	2.8E+12	1.20E+12	71.00	1.01
50	3.5E+12	1.50E+12	72.10	1.03
60	4.2E+12	1.80E+12	72.90	1.04
70	4.9E+12	2.10E+12	73.50	1.05
80	5.6E+12	2.40E+12	74.00	1.05

Table 4 Results increasing axial stiffness for t=800mm model

Multiplication factor axial stiffness	E glass [N/m^2]	E/t int [N/m^3]	Critical displacement of Support. [mm]	Total crit displ as % of span.
1	7.00E+10	1.50E+10	3.20	0.52
10	7.00E+11	1.50E+11	0.32	0.00
20	1.40E+12	3.00E+11	120.16	0.86
40	2.80E+12	6.00E+11	133.28	0.95
60	4.20E+12	9.00E+11	138.77	0.99
80	5.60E+12	1.20E+12	142.04	1.01
100	7.00E+12	1.50E+12	144.26	1.03
120	8.40E+12	1.80E+12	145.87	1.04
140	9.80E+12	2.10E+12	147.06	1.05
160	1.12E+13	2.40E+12	148.04	1.06
180	1.26E+13	2.70E+12	148.80	1.06

It is shown that both models converge to the same value of 1.05% increase of span as the critical support settlement that results in snap-through buckling when the axial stiffness increases. Therefore, it is concluded that when stiffness approaches infinity the critical support displacement (as percentage of the span) becomes independent of scale (basis of chapter 2). The value of 1.05 corresponds to the analytical value found for arches of the same t/l and f/l ratio, as can be observed in the graph in Fig. 2a. As can be expected, a lower axial stiffness results in a lower value for the critical displacement of the support because axial shortening of the arch causes snap-through to occur at a smaller displacement. The FE model indicates that it is important to incorporate the effect of axial stiffness as the estimated 'real' stiffness of the bridge results in snap-through at 0.63% instead of 1.05%.

3.3. Results: Checking the effect of scaling.

To investigate the nonlinear effects of scaling, the model of the TU Delft case-study is again taken as a starting point to determine the ratios t/l and f/l. By keeping the ratios constant the bridge is uniformly scaled. The elasticity of the glass is kept constant at 70GPa. The E/t value for a 1mm sheet of polyurethane has been selected.

To check the effects of scaling with symmetric loading, first only dead load due to the glass itself is applied to the model. Two series have been run. In the first series the interlayer stiffness is inversely scaled to model that a bigger span would result in more bricks and interlayers. In the second series a constant value for E/t is applied to model that a bigger span would result in bigger bricks and an equal number of interlayers. Results are shown in table 5.

Table 5 Results of geometrical scaling. Ratio t/f and t/l and E are kept constant.

t [mm]	f [mm]	l [mm]	Interlayer E/t [N/m3]	Mesh size [m]	Total crit displ as % of span. (scaled E/t)	Total crit displ as % of span (constant E/t)
50	88	1750	2.4E+11	6.25E-03	0.83	0.65
125	219	4375	9.6E+10	1.56E-02	0.77	0.64
200	350	7000	6.0E+10	2.50E-02	0.73	0.64
400	700	14000	3.0E+10	5.00E-02	0.63	0.64
600	1050	21000	2.0^E+10	7.50E-02	0.57	0.63
800	1400	28000	1.5E+10	1.00E-01	0.52	0.63
1000	1750	35000	1.2E+10	1.25E-02	0.46	0.63
1200	2100	42000	1.0E+10	1.50E-02	0.41	0.63
1400	2450	49000	0.8E+10	1.75E-02	0.37	0.62
1600	2800	56000	7.5E+09	2.00E-01	0.33	0.62

To check the effects of scaling on arches with asymmetric loading, a (live) load of 5 kN/m is added to half of the bridge. Again, two series are produced. One with a scaled E/t value and one with a constant E/t value.The results can be seen in table 6.

Table 6 Results scaling with constant asymmetric load.

t [mm]	f [mm]	l [mm]	Interlayer E/t [N/m3]	Mesh size [m]	Total crit displ as % of span. (scaled E/t)	Total crit displ as % of span (constant E/t)
12.5	22	438	9.6E+11	1.6E-03	0.48	-
25	44	875	4.8E+11	3.1E-03	0.51	-
50	88	1750	2.4E+11	6.3E-03	0.54	0.37
200	350	7000	6.0E+10	2.5E-02	0.55	0.47
400	700	14000	3.0E+10	5.0E-02	0.53	0.53
600	1050	21000	2.0E+10	7.5E-02	0.50	0.55
800	1400	28000	1.5E+10	1.0E-01	0.46	0.50
1000	1750	35000	1.2E+10	1.3E-01	0.42	0.59
1200	2100	42000	1.0E+10	1.5E-01	0.38	0.59
1400	2450	49000	8.6E+09	1.8E-01	0.34	0.59
1600	2800	56000	7.5E+09	2.0E-01	0.30	0.58

The results of scaling on snap-through of symmetric and asymmetrisch loaded dry-stacked glass masonry arches as mentioned in the two tables shown before are plotted in Fig. 9. In case of only dead load it is shown that the interlayer stiffness influences the occurance of snap-through. When it is kept constant the critical displacement as percentage of the span is also (almost) constant. When it is scaled the critical displacement reduces when the span increases. In case of asymmetrical loading it can be seen that for large spans the results are similar as for symmetric load. This is due to the fact that the live load scales only in one direction (to the power 1) as opposed to the dead load, which scales in both the direction of the span and the thickness of the arch (to the power 2). The results also show that axial stiffness influences the critical displacement significantly. Axial shortening becomes more relatively more significant as the arch is scaled up. The axial shortening is given by:

$$\Delta l = \frac{F*l}{E*A} \tag{24}$$

In the numerator; scaling of the arch leads to a quadratic scaling of the dead load (the width of 1 m remains constant) which corresponds to a quadratic scaling of the axial force [F]. The length [l] scales linearly. In the denumerator the thickness of the arch, corresponding to [A], scales linearly and the E remains constant. So the axial shortening will scale quadratically, and as Fig. 9 shows, its effect will be more significant when scaling up: the critical displacement of the support becomes subsequently smaller when E/t is also scaled.

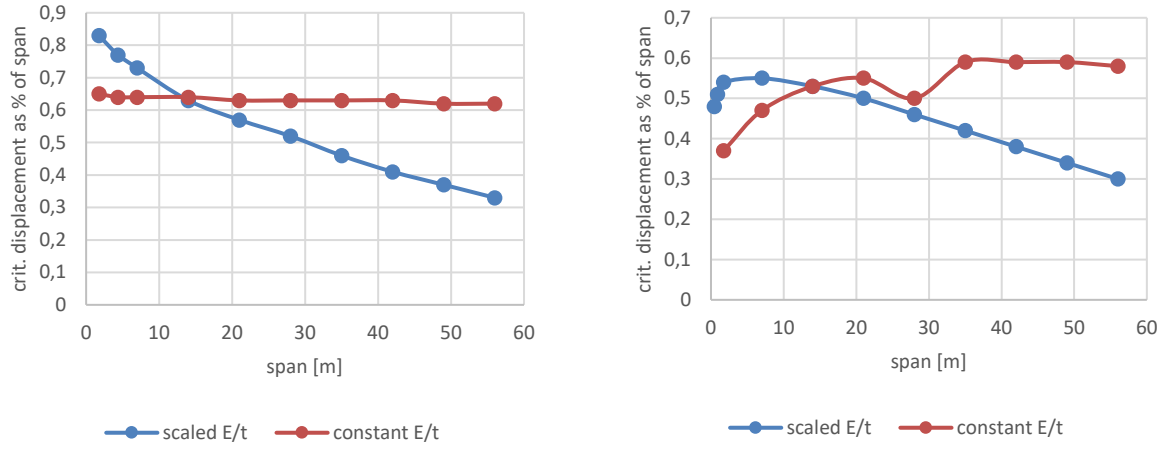

a) b)

Fig. 9 Results from FE analyses; a) Critical displacement when span-through occurs when only dead load is applied; b) Critical displacement when span-through occurs when dead load is applied plus asymmetric live load of 5kN/m.

4. Conclusions

The stability of dry-stacked masonry glass bridges can be analysed both analytically and numerically. Design graphs derived in this paper are based on analytical assesments and can be used in prelimenary arch design. By means of numerical analyses it is shown that significant nonlinear effects influence the stability when axial stiffness is finite. Therefore, axial stiffness is very important to consider during the design which is mainly affected by the choise of interlayer. It is shown that based on stability dry-stacked masonry glass can be designed to span large distances if the geometry is scaled accordingly.

Acknowledgements

We would like to thank the TU Delft and Arup for their time and investments in the research.

References

Gambhir, M.L. (2004). Stability Analysis and Design of Structures, Springer-Verlag, Berlin.
Heyman, J. (1995). The stone skeleton: structural engineering of masonry architecture, Cambridge University Press, Cambridge.
Lomholt, I.: Monumento madrid. https://www.e-architect.co.uk/madrid/atocha-monument-madrid (2007). Accessed 07 January 2017
Oikonomopoulou et al (2016). Challenges in the Construction of the Crystal Houses Façade, Challenging Glass, Ghent.
Oschendorf, J. A. (2002). Collapse of masonry structures, PhD thesis, University of Cambridge, Cambridge.
Snijder, A., Smits, J., Bristogianni, T. and Nijsse, R. (2016). Design and engineering of a dry assembled glass block pedestrian bridge, In Bos et al., Challenging Glass 5 -Conference on architectural and structural applications of glass, Ghent.